Available online at www.sciencedirect.com

jmr&t Journal of Materials Research and Technology

https://www.journals.elsevier.com/journal-of-materials-research-and-technology

Original Article

# Enhancement of pitting corrosion resistance for AA1050 processed by continuous closed die forging

*Sandra L. Rodríguez R.*[a,*], *Jorge H. Díaz A.*[b], *Luis S. Hernández H.*[b], *Francisco G. Pérez-Gutiérrez*[a], *Alexander P. Zhilyaev*[c,d], *Jessica Calvo*[e], *José-María Cabrera*[e,f]

[a] *Department of Mechanical Engineering, Faculty of Engineering, Autonomous University of San Luis Potosi, 78290, Mexico*
[b] *Metallurgy Institute, Autonomous University of San Luis Potosi, 78210, Mexico*
[c] *Laboratory of Mechanics of Gradient Nanomaterials, Nosov Magnitogorsk State Technical University, Magnitogorsk, 455000, Russia*
[d] *Institute for Metals Superplasticity Problems, Ufa, 450001, Russia*
[e] *Department of Materials Science and Metallurgical Engineering, EEBE – Universitat Politècnica de Catalunya, Barcelona, 08019, Spain*
[f] *Institute of Metallurgical and Material Research, Universidad Michoacana de San Nicolás de Hidalgo, Morelia, Michoacán, 58230, Mexico*

ARTICLE INFO

*Article history:*
Received 19 December 2019
Accepted 12 September 2020

*Keywords:*
AA1050
Severe plastic deformation
Mechanical behavior
Pitting corrosion

ABSTRACT

The pitting corrosion of an aluminum alloy AA1050 after being processed by continuous closed die forging (CCDF) was evaluated by cyclic potentiodynamic polarization (CPP). Microstructure evolution, mechanical and corrosion behaviors were studied as a function of the total strain imposed. The CCDF process was carried out at 0, 16 and 24 passes with loading times of 10 and 15 s. The electron backscatter diffraction (EBSD) analysis revealed a grain refinement of 0.78 μm after 24 passes, which promoted an increment in the yield strength (YS), ultimate tensile strength (UTS) and vickers hardness (HV) by a factor of 9, 3 and 2 respectively; but the uniform strain and strain to rupture decreased by 93% and 72% respectively. Resistance to corrosion after 16 and 24 passes was compared with the reference material (0 passes), using CPP in a $Na_2S0_4$ 0.1 mol/l +100 mg/l of NaCl electrolyte. Results showed that the specimens with 24 passes decreased its corrosion rate one order of magnitude. In addition, specimens with very fine grain sizes have shown nobler pitting potential and lower pitting volume fraction than coarse grain specimens.



## 1. Introduction

The first studies about severe plastic deformation (SPD) were carried out by P.W. Bridgman et al. [1–6], who was honored by the Nobel Prize physics in 1946. However, it has been during the last three decades where this processing technique has received large attention by the scientific community. Due to the high strain involved, SPD processes promote grain refinement of the microstructure of a given material, increasing values of mechanical properties, such as hardness, yield strength (YS) and ultimate tensile strength (UTS) [1–5]. An important fact of some SPD techniques is that they can be

* *Corresponding author.*
E-mail: sandyreyna@uaslp.mx (S.L. Rodríguez R.).
https://doi.org/10.1016/j.jmrt.2020.09.065

scaled out to large samples allowing industrial applications [1,4,5,7].

It is well known that the combination of ductility, mechanical strength, low density and formability, makes aluminum an attractive material for structural applications. As well, the application of SPD to aluminum alloys enhances their electrical conductivity, corrosion resistance and so on while increasing their mechanical properties. Most SPD studies on pure aluminum and aluminum alloys have been mainly carried out by equal channel angular pressing (ECAP) and high pressure torsion (HPT) [8]. While results of ECAP in aluminum alloys can be dated in the late 90's, the corresponding ones to modern HPT are relatively recent (early's 2000). Typically, pure aluminum and 1xxx series were preferred in the first studies so no interference with precipitated particles was considered, and only solid solution elements, at the most, was included in those earlier analysis [8–10].

It is also well known that aluminum forms an oxide film on its surface, which acts as a protective layer against environmental corrosion. However, the main disadvantage is its low resistance to pitting corrosion when exposed to halide ions, especially chloride ions [10,11]. Some reviews [8,12] have reported the contradictions found when SPD techniques have been used while studying the resistance to pitting corrosion in aluminum alloys. Such contradictions are attributed [12] to the microstructural changes that occur due to the particular SPD technique used, such as ECAP, high pressure torsion (HPT) and multidirectional forging (MDF) or the passive corrosion rate [8].

Particularly, some authors have concluded that grain refinement increases resistance to corrosion of Al, Mg and its alloys [10,13–16]. For example, Chung et al. [13] obtained an increment of resistance to pitting corrosion of Al1050 after processing via ECAP, where the size of the Si (cathode) impurities was reduced within the Al (anode) die through the number of passes during deformation. Some authors have also pointed out that for a given SPD technique the improvement of resistance to corrosion due to grain refinement is also a function of the processing path used [17].

On the other hand, other researchers working with Al, Al-Mg alloys and pure Mg reported that grain refinement through ECAP promoted a reduced resistance to corrosion [18–21]. They concluded that the increment in corrosion rate was due to accumulation of dislocations originated through the SPD process, the type of protective coating (i.e. its absence at high dissolution rates), the given alloy and the corrosion environment [22].

Resistance to pitting corrosion in samples previously processed by SPD through the ECAP technique has been also studied. Contrary to some other SPD method, ECAP generates a homogenous grain refinement [23]. In parallel, other new SPD techniques have been developed. For instance, continuous close die forging (CCDF) produces ultra-fine grain (UFG) sizes and a bimodal microstructure in opposition to other SPD techniques. This latter technique allows to work with large amount of material, having less complexity than for example the ECAP procedure. However, materials processed by CCDF have not been studied in terms of pitting corrosion.

Given such scenario, and with the aim of providing some new insights in the contradictory results already reported [8,12], this work focuses on studying pitting corrosion on an AA1050 alloy severely deformed by CCDF paying special attention to the size and distribution of the ultrafine grains obtained.

## 2. Materials and methods

### 2.1. *Sample processing using continuous closed die forging (CCDF)*

Four bars of 20-mm in diameter and 100-mm in length were machined from commercial AA1050 (<0.25%wt. Si, <0.40%wt. Fe, Al balance min 99.5%wt. as indicated by the supplier BRONMETAL). In order to homogenize the as-received material, specimens were heat treated as follows: 1) Annealing at 630 °C for 48 h; 2) cooling at 66 °C/h until 300 °C; 3) Annealing at 300 °C for 3 h followed by cooling to room temperature (RT) inside the furnace. This pre-annealing heat treatment has been reported [24,25] to be effective in increasing the yield strength of aluminum alloys after SPD due to the generation of a more homogeneous microstructure. Heat-treated specimens were subjected to CCDF through symmetrical dies with rhomboidal inner cross section. A maximum load of 44 tons was necessary. The deformation process was carried out at RT with loading times of 15 and 10 s at a displacement rate of 5 mm/s. Loading time is expected to affect possible stress relaxation, i.e. recovery and rearrangements of dislocations. So higher loading times promotes more stable dislocation arrangements. Molybdenum disulfide was used as lubricant. In order to quantify the effect induced due to the possible temperature increment, a K-type thermocouple was inserted (by drilling) within the die at just 2 mm below the sample surface. A rough estimation of the temperature increment was obtained with this configuration. The maximum temperature increment measured under continuous operation was 4 °C, which was considered not significant. Table 1 shows nomenclature and experimental parameters for the specimens extracted from the bars.

Each pass of the CCDF consists of two steps (see Fig. 1a). In the first step i) the specimen is placed in the rhomboidal cavity and is longitudinally pressed within the dies; ii) after unloading, the specimen is rotated 90° counterclockwise. In the second step iii) the specimen is again pressed, and iv) the specimen is again rotated 90°. At the end of the CCDF, the specimen acquires a rhomboidal shape with a 15 mm major axis, while the minor axis varies as a function of total number of passes.

Finally, it was found that the load applied during SPD processes must allow permanent strain without compromising the material integrity, such as crack formation. For this reason and to gain understanding of the strain distribution of the specimens after CCDF with 8 passes, a finite element method (FEM) simulation was carried out to predict strains achieved [1]. Such simulation was implemented using DEFORM-3D code. Two regions were identified as illustrated in Fig. 1b: i) the central region with high deformation (HD) with a total strain in the order of 7 had a volume fraction of ~40% of the useful material, and ii) the peripheral region with lower deformation (D) ranging between 1–3. Specimens were extracted from each zone to analyze the total strain effect.

**Table 1 – Description of the experimental parameters used in this investigation.**

| Nomenclature | Number of passes | Processing time (s) | Deformation zone |
|---|---|---|---|
| 0 P | 0 | do not apply | do not apply |
| 16 P | 16 | 15 | Deformed |
| 16 PHD | 16 | 15 | Highly Deformed |
| 24 P | 24 | 15 | Deformed |
| 24 PHD | 24 | 15 | Highly Deformed |
| 24 P* | 24 | 10 | Deformed |
| 24 PHD* | 24 | 10 | Highly Deformed |

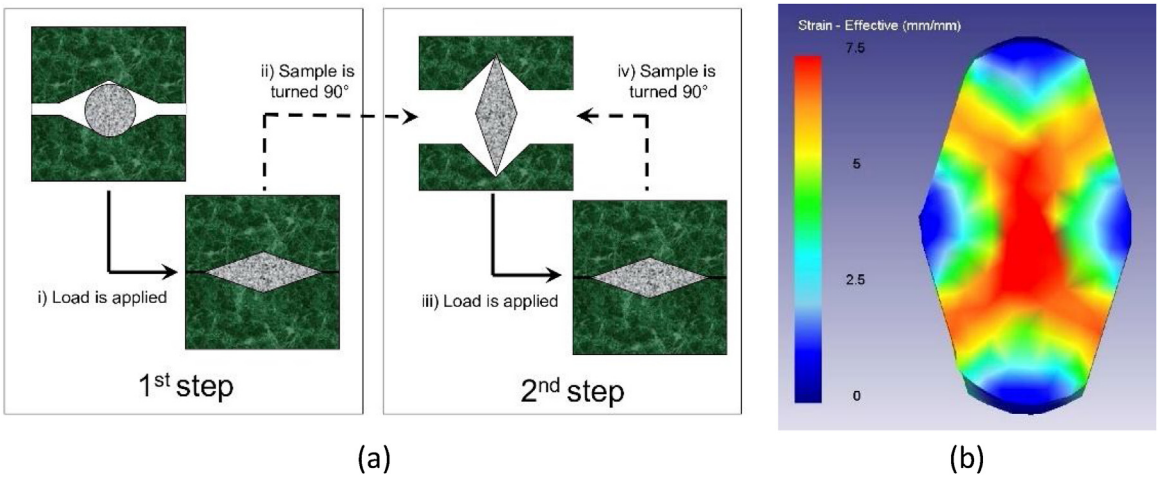


**Fig. 1 – (a) Scheme of the sequence in the CCDF process. (b) Distribution map of Effective Plastic Deformation (EPD) simulated by FEM (8 passes of CCDF).**

### 2.2. *Microstructure and mechanical properties*

After CCDF, specimens were prepared by standard metallographic procedures for observation and interpretation. For this purpose, the grain size and misorientation distribution were obtained through electron backscatter diffraction (EBSD) technique using a scanning electron microscopy (SEM) Jeol JSM-5600. From the 100 mm bar, three 10 mm thick discs were removed along the longitudinal section at 10, 50 and 90 mm for the microindentation tests, which were carried out based on the Vickers scale with a 4-sided pyramidal microdurometer (AKASHI-HO).

Due to the dimensions of the bars, four tensile test specimens with total length of 45 mm, nominal diameter (D) of 5 mm, the gauge length (G) of 20 mm, length of reduced section (A) of 20 mm and radius of fillet (R) of 1.5 mm, were extracted from the longitudinal axis of the central region of the CCDF processed specimen (Fig. 2). These samples were tested until failure using a universal testing machine (INSTRON 4507) at a strain rate of 0.001 $s^{-1}$.

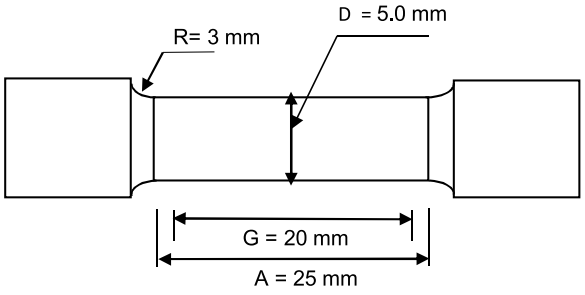


**Fig. 2 – Dimensions in tensile test specimen.**

### 2.3. *Corrosion tests*

In the case of corrosion tests, specimens were extracted by saw cutting and then polished up to sand paper grit 1200. Then they were encapsulated in cold setting polyestirene resin. To minimize the effects of possible grooves between the specimens and the resin, the specimen surface was covered with adhesive tape, leaving a 0.107 $cm^2$ surface area exposed to the electrolyte. Corrosion tests were carried out at RT.

The cyclic potentiodynamic polarization (CPP) technique was used to evaluate the resistance to localized corrosion due to pitting. Open circuit potential (Eoc) evolution was registered within a 0.1 mol/l of $Na_2SO_4$ electrolyte to which 100 mg/l of NaCl were added. It is well known that such solution promotes pitting corrosion. The experiments were carried out with no deaerated electrolyte under pH = 5. The CPP curves were obtained after 480 s of contact with the electrolyte. Potentiodynamic measurements at a scanning rate of 0.166 mV/s were initiated with a cathodic potential value of 250 mV with respect to the Eoc and rising scanning until a current density of 1 mA/$cm^2$, when the scanning was inverted. A saturated calomel electrode (SCE) and two high density graphite bars were used as reference and auxiliary electrodes respectively.

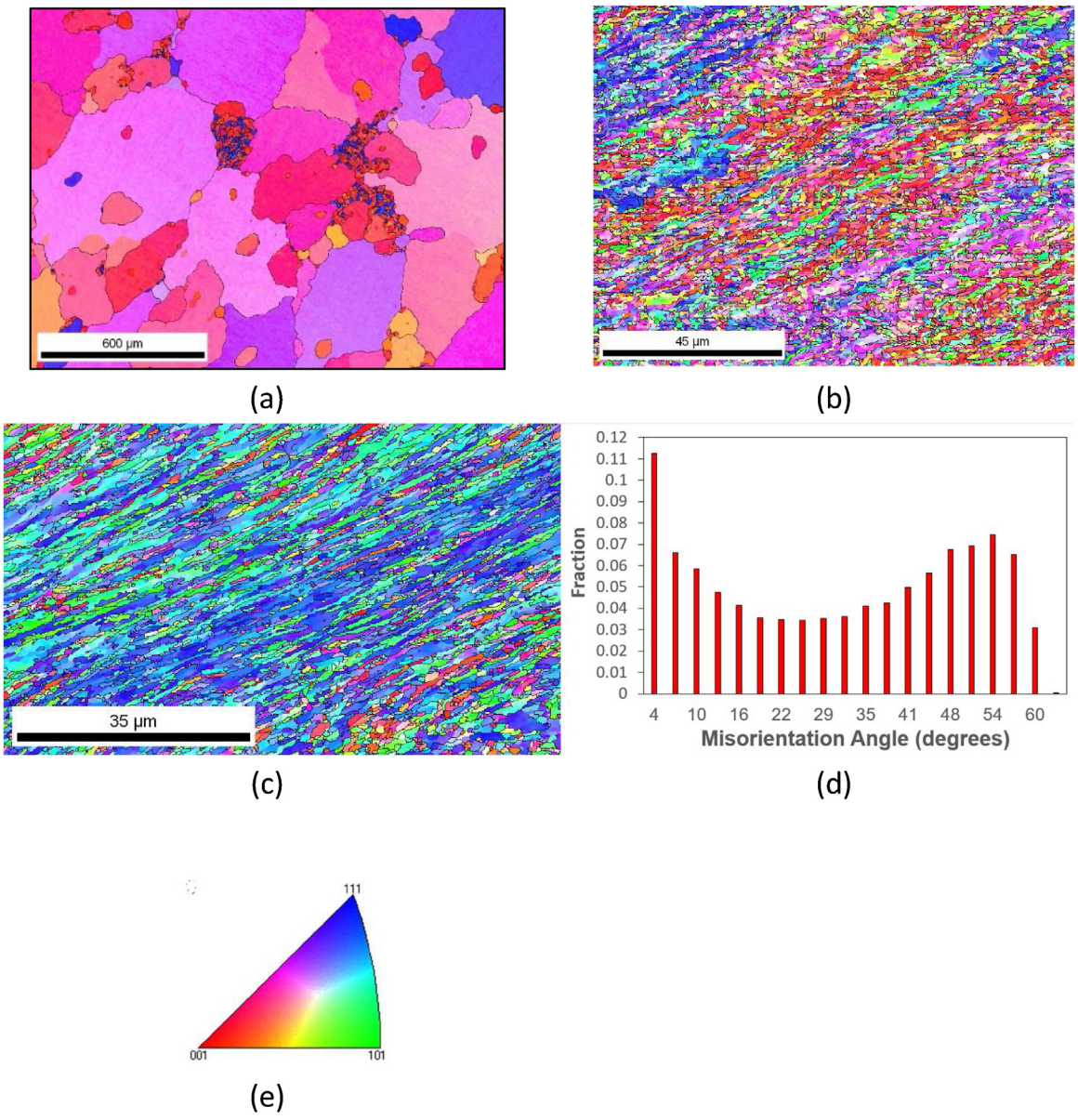


**Fig. 3 – Evolution of the grain size for samples (a) 0 P, (b) 16 P and (c) 24 P of AA1050 processed via CCDF. (d) Grain boundary misorientation distribution of sample 24 P. (e) Inverse pole figure colour code.**

Reproducibility of results was confirmed with a minimum of two specimens for each condition. The criterion for the fitting parameters was the lowest value for $Chi^2$. Regarding the method used for computing corrosion current density ($i_{corr}$) and corrosion rate (CR), from the obtained polarization curve for each material, the anodic and cathodic Tafel slopes, βa, and βc respectively, and the $i_{corr}$ were calculated using the Echem Analysit 5.56 software available on the potentiostat used. While the CR in thousandths of an inch per year (mpy) was calculated from the expression CR (mpy) = 0.129 Mi/nD [26], where M is the atomic weight of Al, i is the corrosion current density in $\mu A/cm^2$, n the number of electrons transferred and D the density of Al in $g/cm^3$.

Because the microstructure of the bars deformed via CCDF is not homogenous (see Fig. 1b), the specimens extracted from the bars were treated with Keller reactant to have confidence that the experiments were carried out in different deformation regions. The samples were cut until the pitting originated by the reactant was removed. Later, a surface preparation was carried out through sandpaper. In a parallel study [1,25], a deeper mechanical analysis was carried out, and results indicated that there was no strong influence of the direction of sample extraction, so a rather isotropic microstructure was assumed and, consequently, it is speculated that corrosion results are also isotropic.

## 3. Results and discussion

### 3.1. *Microstructure evolution*

Figs. 3(a) to 3(c) show the EBSD texture maps for the specimens 0 P, 16 P and 24 P while Fig. 3(d) displays the misorientation angle distribution of the 24 P specimen. Fig. 3(a) illustrate a

heterogeneous microstructure formed by uniaxial grains with an average size of ~150 μm, together with some few large (~600 μm) grains. Specimen 16 P in Fig. 3(b) shows a much more refined grain size compared with specimen 0 P. The average grain size is ~1 μm with a mixed elongated and uniaxial morphology. In turn, sample 24 P (Fig. 3c), displays a smaller average grain size close to 0.78 μm with a similar morphology to the 16 P specimen although more elongated. Additionally, the grain size aspect ratio, longitudinal/transverse dimensions in the specimen cross section after 24 P was approximately 2.5. It is also evident that after 24 P a different texture is noticed, as most grains are oriented into the <111> direction while after 16 passes the texture was more oriented towards <001>. Fig. 3(d) exhibits the grain boundary misorientation distribution of the sample processed after 24 passes. It must be mentioned that grain boundaries with misorientation angle higher than 15° are considered as a high angle grain boundary (HAGB) and when such angle is lower than 15°, they are considered a low angle grain boundary (LAGB). One can readily notice that the misorientation angle distribution shows a bimodal configuration, with a HAGB fraction near to ~62%. This means that there is still some potential for further grain refinement, as 38% of the boundaries can still become HAGB. This also means that the grain size has not yet attained a steady state as expected in many SPD processes after certain amount of strain. This steady state depends also on the deformation mode, and the current observation would indicate that CCDF is less efficient in refining the microstructure than ECAP, in the sense that more strain must be introduced by CCDF than in ECAP to achieve similar grain sizes.

Finally, it must be mentioned that second phase of particles or inclusions were not observed while preparing the samples for the EBSD examination. In consequence the possible effect of the type, size and distribution of second phase in pitting corrosion was not considered.

### 3.2. *Mechanical properties*

Table 2 shows the results of mechanical properties as HV, YS, UTS and elongation, together with grain size of the current aluminum alloy processed via CCDF and two commercial purity aluminums processed by ECAP [19,26]. In general, the YS and UTS values in the CCDF samples incremented with the number of passes and the loading time. It is remarkable that the YS increases by a factor of 9 for the 24 PHD specimens with 15 s of loading time, with respect to the 0 P specimen. Similarly, HV increases by a factor of ~2. Regarding the difference in the behavior of the processed material after loading times of 15 and 10 s, it is expected that the increase in this loading time will avoid stress relaxation, that is, recovery from dislocation and, therefore, promote a more stable arrangement of dislocations. The 24 PHD* specimen with 10 s of loading time, presents values of 170 and 208 MPa for YS and UTS respectively. These values are slightly lower than those obtained for 24 PHD as expe4cted. While for the 16 PHD specimen, a YS of 170 MPa and a UTS of 190 MPa were obtained.

It should be mentioned that although total elongation was relatively large ranging from 18% to 24%, the uniform elongation, the one needed for further processing or in service behavior, was very small in all ECAP samples and lower than to

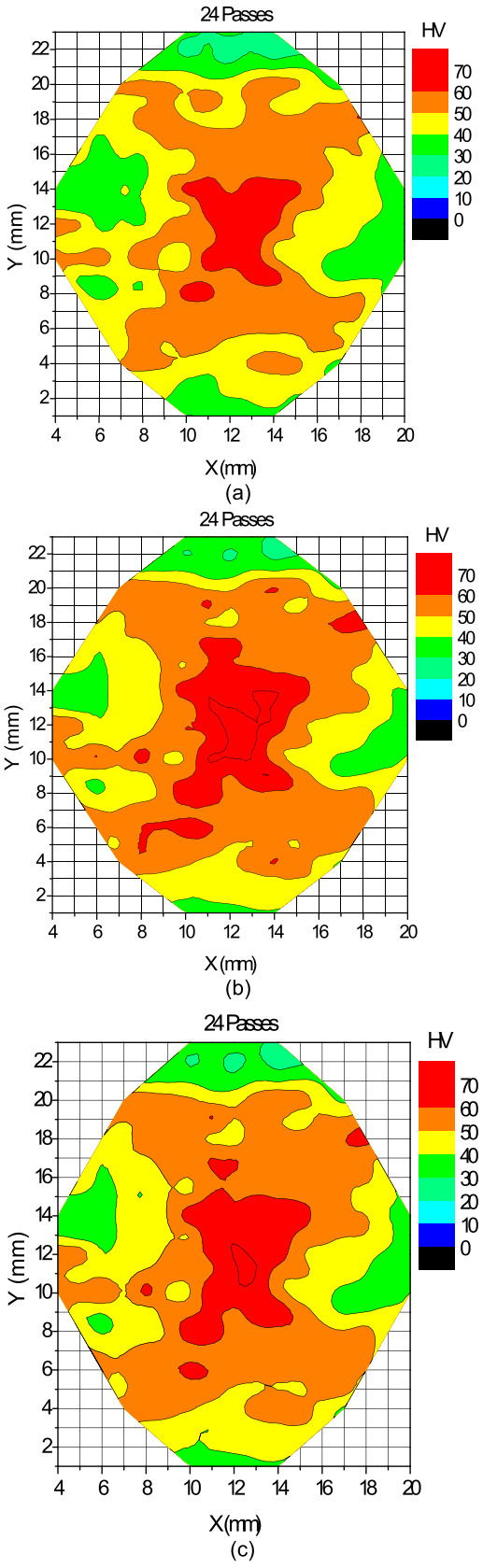


**Fig. 4 – Hardness profile evaluated at (a) 10, (b) 50 and (c) 90 mm along the longitudinal section.**

**Table 2 – Microstructure and mechanical properties of aluminium alloys processed by CCDF and ECAP [19,25,26].**

| Sample | Grain size (μm) | HV | YS (MPa) | UTS (MPa) | Uniform elongation (%) | Elongation to rupture (%) |
|---|---|---|---|---|---|---|
| 0 P [25] | 400 | 28 ± 2 | 20 | 70 | 44 | 66 |
| 16 PHD [25] | 1 | 60 ± 5 | 170 | 190 | 4 | 19 |
| 24 PHD* [25] | 0.78 | 62 ± 3 | 170 | 208 | 3 | 18 |
| 24 PHD [25] | | 62 ± 2 | 180 | 226 | 3 | 18 |
| ECAP 4 P [19] | 0.19 | 51 ± 2 | 135 | 160 | – | 24 |
| ECAP 10 P [26] | 0.3 | 60 ± 2 | 160 | 200 | – | 18 |

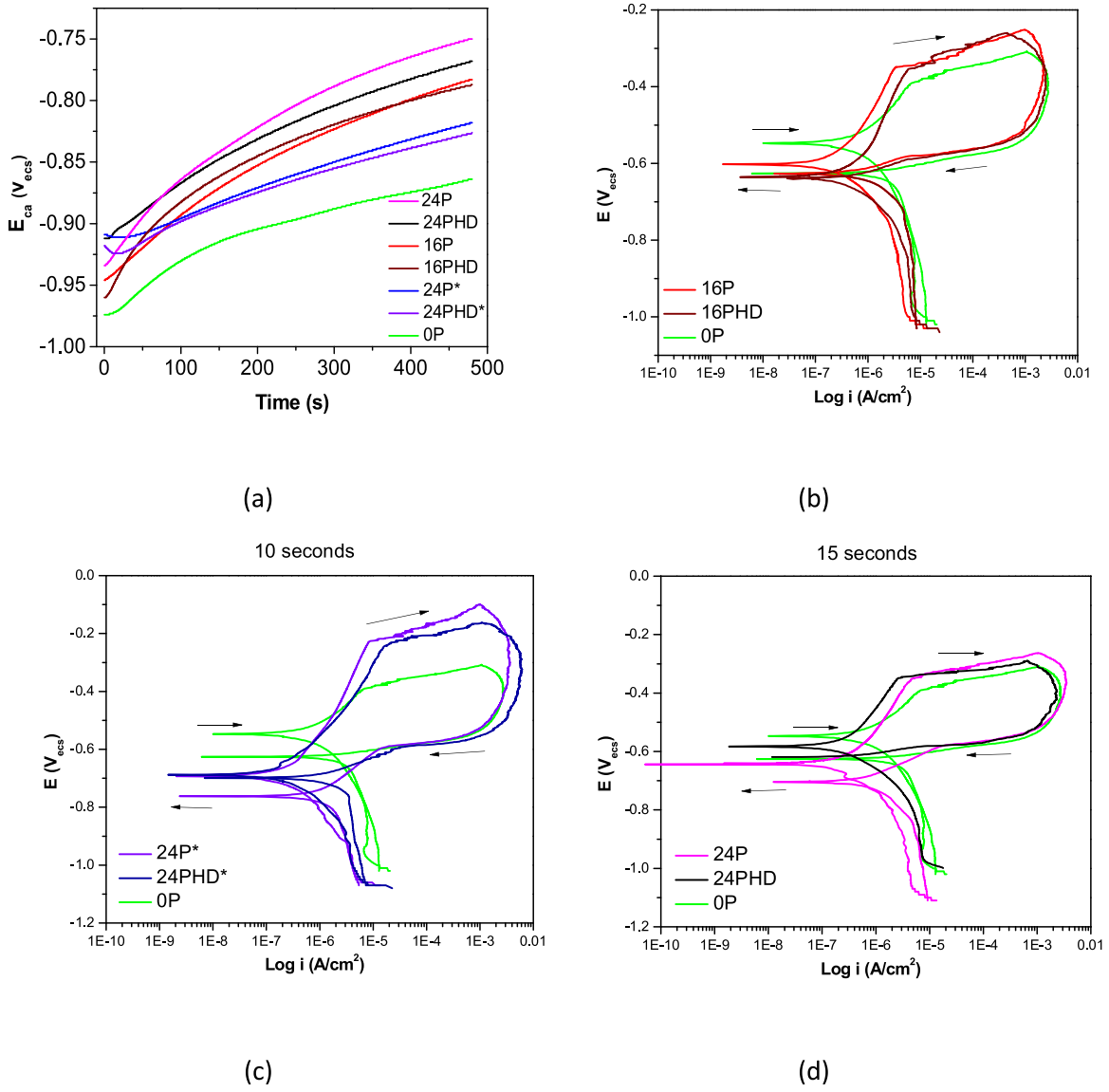


**Fig. 5 – (a) Typical evolution of $E_{oc}$ with respect to time for AA1050 processed via CCDF after 0, 16 and 24 passes.**

2.5% [1,25]. For the 24 PHD specimen, the uniform strain and strain to rupture decreased by 93% and 72% respectively, as has been found in other works [1,19,25,26].

The applied pressure upon die closure produces and effective strain over the specimen's cross section, while the longitudinal section remains constant: with that, the constant volume requirement of SPD is fulfilled. To evaluate that mechanical behavior over the longitudinal section, three specimens were extracted from the bar, where measured mechanical properties resulted with not significant variations (Fig. 4). The average hardness of the three specimens extracted was 60 ± 5 HV. This confirmed the homogeneity of the mechanical properties across the longitudinal section. It is worth mentioning that the volume fraction with high hard-

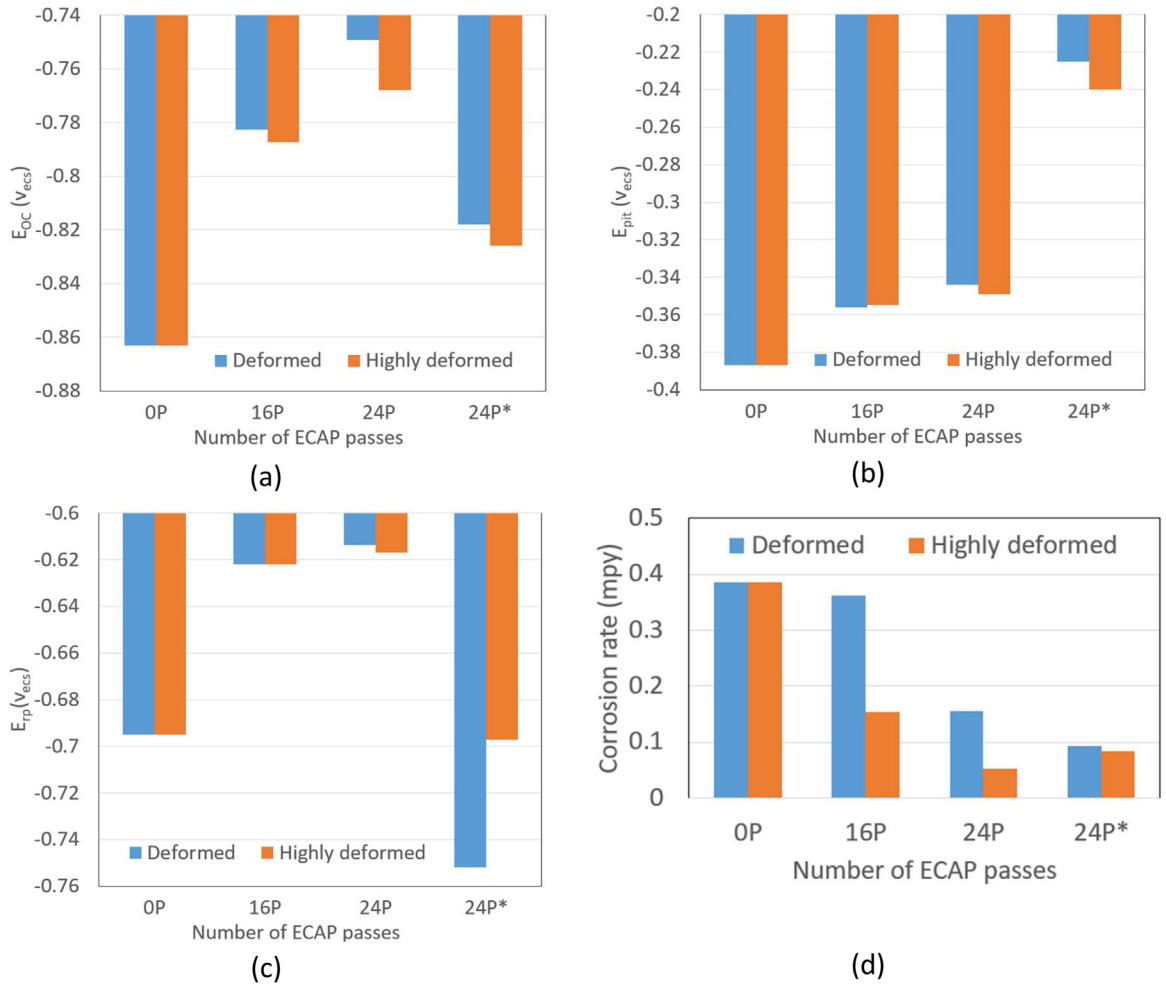


**Fig. 6 – Influence of the number of CCDF passes and the amount of strain on: (a) open circuit potential ($E_{oc}$), (b) pitting corrosion potential ($E_{pit}$), (c) repassivation potential ($E_{rp}$) and (d) corrosion rate.**

**Table 3 – Values of $E_{oc}$ and electrochemical parameters calculated from the CPP.**

| Sample | $E_{oc}$ (V) | $\beta_a$ (V/decade) | $\beta_c$ (V/decade) | $i_{corr}$ (nA/cm$^2$) | Corrosion rate (mpy) | Chi$^2$ |
|---|---|---|---|---|---|---|
| 0 P | −0.863 | 0.163 | 0.181 | 890 | 0.385 | 3.37e$^{-8}$ |
| 16 P | −0.782 | 0.293 | 0.127 | 835 | 0.362 | 4.20e$^{-8}$ |
| 16 PHD | −0.787 | 0.366 | 0.183 | 354 | 0.153 | 3.66e$^{-8}$ |
| 24 P | −0.749 | 0.063 | 0.075 | 357 | 0.155 | 4.34e$^{-8}$ |
| 24 PHD | −0.768 | 0.236 | 0.265 | 121 | 0.052 | 9.87e$^{-10}$ |
| 24 P* | −0.818 | 0.151 | 0.132 | 212 | 0.092 | 6.68e$^{-9}$ |
| 24 PHD* | −0.826 | 0.195 | 0.106 | 193 | 0.084 | 4.42e$^{-8}$ |

ness and strength parameters obtained for the 24 PHD samples with 10 and 15 s was 58% and 60% respectively.

It is worth noticing that similar results in terms of mechanical properties are obtained irrespective of the SPD technique applied, whether CCFD or ECAP, even though the grain sizes are different.

This means that, for the longitudinal section, it is shown by the hardness profiles of Fig. 4, that the mechanical properties relative to each point of the cross section (with a respective degree of deformation) are similar to along the entire length of the bar. For this reason, it was assumed that the corrosion parameters would have a similar behavior to the mechanical properties and therefore, it was decided to measure these parameters in the cross section.

### 3.3. *Effect of the number of passes in the CCDF process on the corrosion resistance*

Fig. 5(a) shows the $E_{oc}$ measurements when the AA1050 specimens were processed with different passes of CCDF. It is observed that at the onset of immersion, the negative $E_{OC}$ values increased rapidly to anodic values; such increment is related to the formation of a passive layer [27]. The 0 P specimen shows the lowest potentials, followed by the speci-

**Table 4 – Experimental parameters in this research in comparison with other authors [18,24].**

| Reference | Material-SPD | Number of passes | Grain size initial/final (μm) | % of grain refinement |
|---|---|---|---|---|
| ECAP [18] | AA1060 | 0P | 80 | 99.76% |
| | | 4P | 0.19 | |
| ECAP [24] | AA1080 | 0P | 390 | 99.92% |
| | | 10P | 0.3 | |
| CCDF [current work] | AA1050 | 0P | 150 | 99.48% |
| | | 24PHD | 0.78 | |

mens with 10 s loading time. The specimens with 15 s loading time have more anodic potentials as the number of passes increases. In all cases the curves show fluctuations related to the activation and repassivation, i.e., the onset and sealing of metastable pitting [28]. Regions with different deformation levels show insignificant $E_{oc}$ changes with the number of passes, whereas the regions with high deformation show more negative potentials.

Fig. 5(b), (c) and (d) shows the CPP results. All the specimens show similar behavior, with well-defined passive region and pitting corrosion potential ($E_{pit}$). $E_{pit}$ represents the potential at which pitting occurs during the initial scan while the current increases abruptly.

Typical CPP curves after 480 s of contact with the electrolyte with (b) 16 passes, (c) 24 passes (10 s) and (d) 24 passes (15 s).

Moreover, all specimens show a large positive hysteresis cycle, which is often an indication of poor resistance to pitting because the film was damaged when the potential was increased within the passive region of the CPP curve, where the regeneration will be difficult. Curves corresponding to the 24 P* are remarkably over all others.

A simple way to analyze the information from the CPP curves is through the variation of the electrochemical parameters obtained from such curves with respect to the number of passes as shown in Fig. 6, together with variations of $E_{oc}$ and corrosion rate, in mpy. As shown in Fig. 6(a), the $E_{oc}$ of CCDF processed specimens became nobler as the number of passes increases and with longer loading times.

These nobler potentials are an indication of a better thermodynamic ability of the refined microstructures to resist corrosion [17]. The difference between both deformation regions is small. In Fig. 6(b), both loading times and deformation regions show nobler $E_{pit}$ than the 0 P specimen. It has been identified that differences below 50 mV in $E_{pit}$ are negligible [29]. For the AA1050 specimens with 15 s of loading time, the $E_{pit}$ differences are below 50 mV, even for the 0 P specimen. In contrast, for the 10 s loading time such differences are ~100 mV. As illustrated in Fig. 6(c), values of the repassivation potential ($E_{rp}$) increase with the number of passes for the 15 s loading time specimens, while it remains constant for the specimens with 10 s of loading time. Finally, corrosion rate of all specimens treated by CCDF decreases with the number of passes with respect to the 0 P specimen as shown in Fig. 6(d).

It is accepted that when the $E_{pit}$ value is nobler, the metallic material will better resist the pitting formation and the potential will passive more easily. Therefore, it is desirable that a material has both potentials, $E_{oc}$ and $E_{pit,}$ as high as possible. It has been proposed that if a series of metallic materials, like

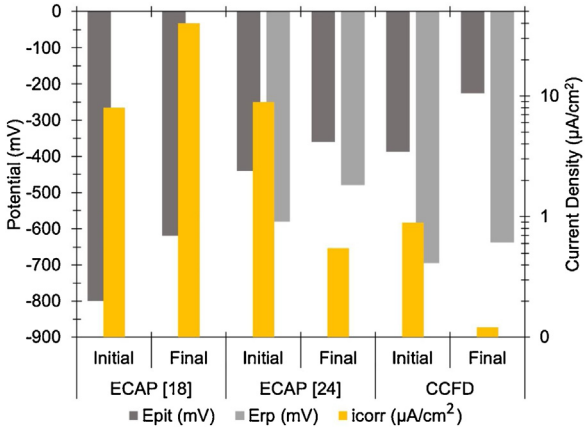


**Fig. 7 – $E_{pit}$, $E_{rp}$ and $i_{corr}$ in this research in comparison with other authors [18,24].**

the one in this study, is tested under similar conditions, the susceptibilities relative to pitting corrosion can be determined by comparing the size of the hysteresis cycle, even though a good approximation is to measure $E_{pit}$-$E_{rp}$ instead of the area enclosed by hysteresis cycle [30]. Fig. 5 shows that specimens with 10 s loading time present larger hysteresis cycles enclosing all other curves, because its $E_{pit}$ is nobler and its $E_{rp}$ more negative, which indicates behaviors with opposite effects.

As it has been pointed out, the large hysteresis cycles are indicative of a poor resistance to localized attack. It should be recalled that the absolute values of these parameters do not depend on the material properties only, but also on the experimental conditions, such as current density, scanning rate, temperature, etc. For example, in this work the initial scan was carried out up to a current density of 1 mA/cm$^2$ while in another study [25] the same scan was carried out up to only 0.1 mA/cm$^2$ (Al1080 in a 3.5% NaCl solution at 2.0 mV/s), with which the hysteresis cycles were very narrow. The reason is that the $E_{rp}$ value is determined by the amount of previous damage to the passive surface. The further the polarization is generated in the anodic direction, the greater the degree of alteration of the surface region [31]. With respect to the scanning rate, within the range of 5–100 mV/s, the $E_{pit}$ is displaced to nobler values [19]; it is worth to mention that the scanning rate in this work was 0.166 mV/s. Table 3 shows the values of electrochemical parameters. In all CCDF treated specimens, current density ($i_{corr}$) is lower than in the 0 P specimen. Such values are in the order of nA/cm$^2$ and corrosion rate is lower for specimens with high deformation (HD). There are differ-

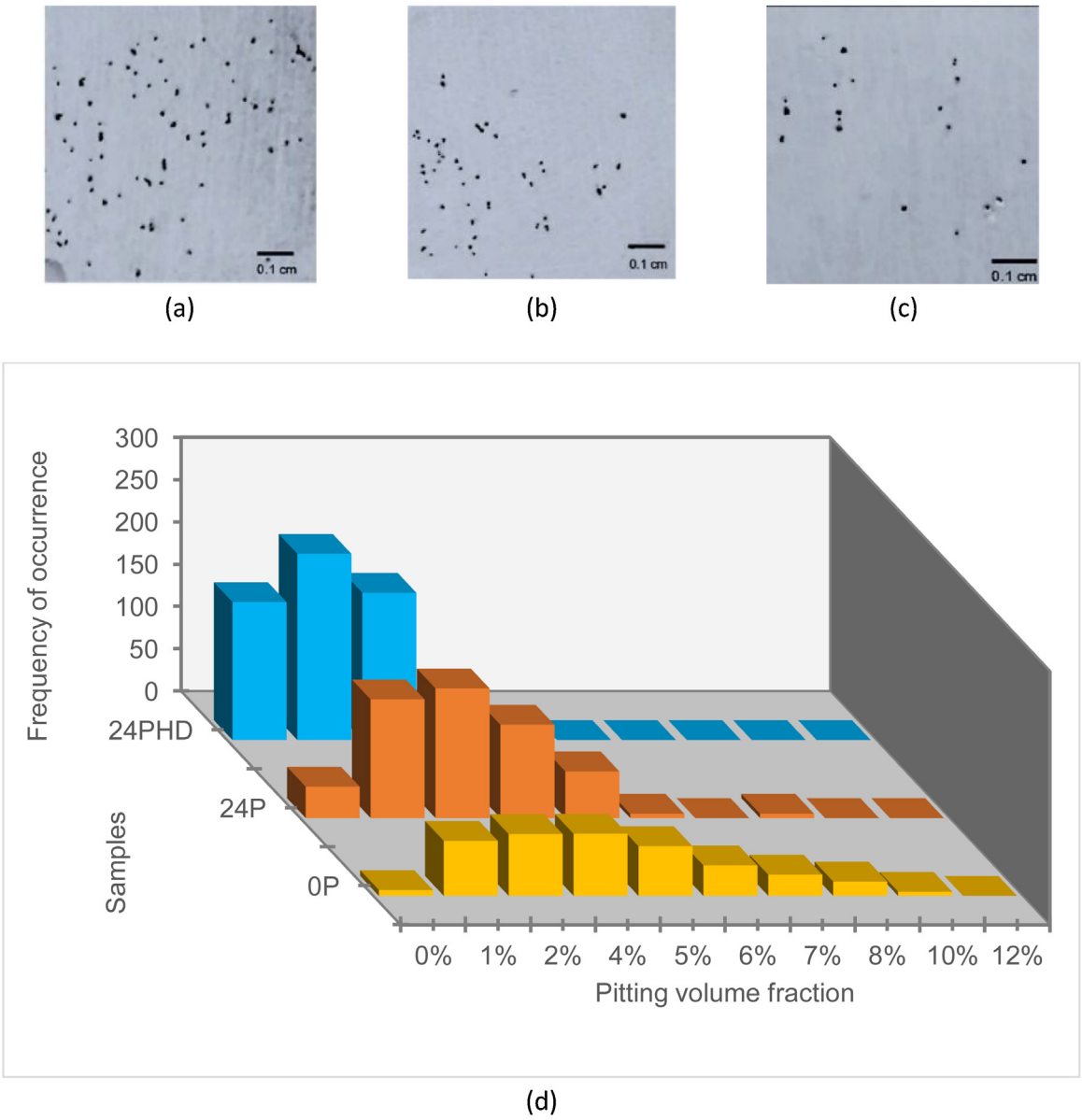


**Fig. 8 – Evolution of pitting corrosion for samples (a) 0 P, (b) 24 P and (c) 24 PHD. (d) Results obtained for the pitting volume fraction and frequency of occurrence of pitting corrosion for samples 0 P, 24 P and 24 PDH.**

ent reasons for the decrease of $i_{corr}$ of ultra fine grain (UFG) AA1050 and AA1080. For AA1050 [10], the high density of grain boundaries and dislocations offers sites that facilitate formation of more dense passive films, while the inner residual tension keep the passive film stable and full, in contrast with a coarse grain material. For AA 1080 [25], the decrease in grain size and latter impurities dispersion were responsible for the increment in the resistance to corrosion. In the same way, it is reported that the high fraction of grain boundaries in the microstructure reduces the $i_{corr}$, accelerating the passivation process and reducing the galvanic couple intensity between the inner part of the grain and its boundary. This is confirmed by the EBSD study in Fig. 3(d), where it is observed that a HAGB fraction around ~62% promoted that corrosion rate values decreased for this work.

At this initial stage of the study, improvement in the $i_{corr}$ may be attributed to: i) A very fine grain size was achieved as a consequence of CCDF in 24 P specimens. ii) A large HAGB fraction, high dislocation density and residual tension and improved localized resistance to corrosion which occurs due to the difference of precipitates [32,33]. iii) A binomial distribution in the HAGB and LAGB fractions was found, which generates the formation of grains and subgrains, producing differences in the energy stored in the microstructure between regions with different levels of deformation [32,33]. However, further investigation is necessary to determine exactly what caused the uniform and localized decrease in corrosivity.

Table 4 shows experimental parameters for different investigations using ECAP and CCDF for Al alloys. It is observed that all specimens achieved a grain refinement when SPD tech-

niques were applied, obtaining an average grain refinement value around ~99%.

In a previous work, Korchef et al. [19] observed that $i_{corr}$ increases after applying ECAP, attributing this loss in the corrosion resistance to the decomposition of the supersaturated solid solution and formation of nano-precipitates. Nevertheless, it is important to mention that in such work [19], the total strain is small compared with those in this work and by Abd El Aal et al. [26].

Fig. 7 shows electrochemical parameters: $E_{pit}$, $E_{rp}$ and $i_{corr}$. Where it is observed that all the $E_{pit}$ and $E_{rp}$ values become nobler or anodic after the SPD technique applied.

As a consequence, a HAGB above 62% was observed for this work and for Abd El All et al. [26], while Korchef et al. [19] only present results of dislocation density without confirming the formation of HAGB. In contrast, Abd El All et al. [26] report a decrement in $i_{corr}$ in samples after 10 ECAP passes. These authors suggest that such improvement is due to the fact that refinement of the microstructure with the number of passes produces the formation of electrochemical batteries with closed spaces in anodic and cathodic regions. In this investigation, as well as in [26], a decrement in the $i_{corr}$ starting with values higher than 1 $\mu A/cm^2$ and finishing with values below 0.1 $\mu A/cm^2$ were noticed as listed in Table 4 and Fig. 7.

After the CPP experiments, pitting was visually confirmed on the surface of all the specimens. A quantification of volume fraction occupied by the pitting was carried out according to the ASTM E562. Fig. 7 shows the evolution of pitting corrosion for the (a) 0 P, (b) 24 P and (c) 24 PHD specimens. A positive result is that increasing SPD through CCDF produces an increment in the resistance to pitting corrosion, where the specimen with less corrosion was the 24 PHD. As pointed out in other studies [15,25], the amount of pitting in a region without deformation with large grains is larger compared to that in ultra fine grains regions. The greater the deformation degree, the less the amount of pitting [11,15,25], confirming the results shown n Fig. 8(a), 6(b) and 6(c). It should be noticed that there is a significant difference between the specimens with CCDF treatment and the 0 P specimen, where the latter presents a larger amount and size of pitting. Fig. 8(d) confirms the visual results by plotting the pitting volume fraction and the frequency of occurrence for the 0 P, 24 P and 24 PHD samples. Again the 24 PHD specimen shows the lowest percentage of pitting volume fraction, which ranged 2.46% $\pm$ 0.244% while the 24 P and 0 P specimens show values of 2.78% $\pm$ 0.276% and 4.05% $\pm$ 0.398% respectively.

## 4. Conclusions

i) The CCDF process has been used to obtain a large grain size refinement in AA1050 specimens. When the number of passes increases and the load is applied during 15 s, the grain size is reduced from 150 to 0.78 μm with respect to the reference specimen. In addition, the grain refinement increased the values of UTS, YS and hardness by a factor of 3, 9 and 2 respectively. Total elongation ranged 18–24 % while uniform elongation was as low as 2.5%. The corrosion rate decreased by 87% for the 24 P specimen with respect to the 0 P specimen.

ii) The open circuit potential ($E_{oc}$) of AA1050 changed to nobler or anodic values with increasing number of passes by CCDF.

iii) A reduction of the $i_{corr}$ was achieved in the microstructure refined by CCDF.

iv) The specimens processed by CCDF exhibited lower pitting volume fractions than the microstructure of the coarse grain specimen (0 P) by approximately 50%.

v) The CCDF treatment increases the mechanical properties and corrosion resistance of the material specially to pitting corrosion. In this work, as in refs. [25,32], it was found that a highly deformed microstructure produces an improvement in the corrosion resistance possibly due to the reduction of $i_{corr}$, the acceleration of the passivation process observed from the evaluation of the open circuit potential ($E_{oc}$), pitting corrosion potential ($E_{pit}$), repassivation potential ($E_{rp}$) and corrosion rate, as well as in the reduction of the pitting corrosion volume fraction.

It is worth mentioning that, although the objective of this study was to demonstrate that it is possible to improve the corrosion resistance response through a new SPD technique, for future work it is important to carry out the evaluation of the passive layer.

## Conflict of interest

The authors declare no conflicts of interest.

## Acknowledgments

A.P. Zhilyaev gratefully acknowledges financial support from the Ministry of Education and Science of the Russian Federation (Grant 14.Z50.31.0043). S.L. Rodríguez-Reyna thanks financial support from Consejo Nacional de Ciencia y Tecnología (CONACyT México) for the grant with CVU 929098. J.M. Cabrera also thanks CONACyT for its partial funding of his sabbatical leave in UMSNH. Authors also thank the technical support in the corrosion tests provided by Martha Alejandra Lomeli, from the Metallurgy Institute of UASLP.

## REFERENCES

[1] Zhilyaev AP, Rodriguez S, Calvo J, Cabrera JM. Novel method of severe plastic deformation–continuous closed die forging: CP aluminium case study. Defect Diffus Forum 2018;385:302–7, http://dx.doi.org/10.4028/www.scientific.net/DDF.385.302.

[2] Kommel L, Shahreza BO, Mikli V. Microestructure and physical-mechanical properties evolution of pure tantalum processed with hard cyclic viscoplastic deformation. Int J Refract Metals Hard Mater 2019;83:104983, http://dx.doi.org/10.1016/j.ijrmhm.2019.104983.

[3] Qian XG, Starink MJ, Gao N. Hardness inhomogeneity and local strengthening mechanisms of an Al1050 aluminium alloy after one pass of equal channel angular pressing. Mat Sci Eng A 2009;513:52–8, http://dx.doi.org/10.1016/j.dt.2016.01.013.

[4] Jing A, Ke-shi Z, Hwai-Chung W, Mei-hua Y. Experimental and numerical investigation on pure aluminium by ECAP.

Trans Nonferrous Met Soc China 2009;19:1303–11, http://dx.doi.org/10.1016/S1003-6326(08)60442-2.
[5] Xu C, Horita Z, Langdon TG. Microestructural evolution in an aluminium solid solution alloy processed by ECAP. Mat Sci Eng A 2011;528:6059–65, http://dx.doi.org/10.1016/j.msea.2011.04.017.
[6] Dan S, Ai-bin M, Jing-Hua J. Corrosion behaviour of ultra-fine grained industrial pure Al fabricated by ECAP. Trans Nonferrous Met Soc China 2009;19:1065–70, http://dx.doi.org/10.1016/S1003-6326(08)60407-0.
[7] Langdon TG. Twenty-five years of ultrafine-grained materials: achieving exceptional properties through grain refinement. Acta Mater 2013;61(19):7035–59, http://dx.doi.org/10.1016/j.actamat.2013.08.018.
[8] Sabirov I, Yu Murashkin M, Valiev RZ. Nanostructured aluminium alloys produced by severe plastic deformation. New horizons in development. Mat Sci Eng A 2013;560:1–24, http://dx.doi.org/10.1016/j.msea.2012.09.020.
[9] Vishnu P, Raj Mohan R, Krishna Sangeetha E, Raghuraman S, Venkatraman R. A review on processing of aluminium and its alloys through Equal Channel Angular Pressing die. Mater Today Proc 2019:1–11, http://dx.doi.org/10.1016/j.matpr.2019.04.223.
[10] Abdulstaar M, Mhaede M, Wagner L, Wollmann M. Corrosion behaviour of 1050 severely deformed by rotary swaging. Mater Des 2014;57:325–9, http://dx.doi.org/10.1016/j.matdes.2014.01.005.
[11] Ezuber H, El-Houd A, El-Shawesh F. A study on the corrosion behavior of aluminum alloys in seawater. Mater Des 2008;29:801–5, http://dx.doi.org/10.1016/j.matdes.2007.01.021.
[12] Miyamoto H. Corrosion of ultrafine grained materials by severe plastic deformation. An Overview Mat Trans 2016;57:559–72, http://dx.doi.org/10.2320/matertrans.M2015452.
[13] Chung M-K, Choi Y-S, Kim J-G, Kim Y-M, Lee J-C. Effect of the number of ECAP pass time on the electrochemical properties of 1050 Al alloys. Mater Sci Eng A 2004;366:282–91, http://dx.doi.org/10.1016/j.msea.2003.08.056.
[14] Dolega L, Adamczyk-Cieslak B, Mizera J, Kurzydlowski KJ. Corrosion resistance of model ultrafine-grained Al-Li alloys produced by severe plastic deformation. J Mater Sci 2012;47:3026–33, http://dx.doi.org/10.1007/s10853-011-6133-0.
[15] Nakano H, Yamaguchi H, Yamada Y, Oue Satoshi, Son In-Joon, Horita Zenji, et al. Effects of high-pressure torsion on the pitting corrosion resistance of aluminum-iron alloys. Mater Trans 2013;54:1642–9, http://dx.doi.org/10.2320/matertrans. MH201301.
[16] Brunner JG, Birbilis N, Ralston KD, Virtanen S. Impact of ultrafine-grained microstructure on the corrosion of aluminium alloy AA2024. Corr Sci 2012;57:209–14, http://dx.doi.org/10.1016/j.corsci.2011.12.016.
[17] Argade GR, Panigrahi SK, Mishra RS. Effects of grain size on the corrosion resistance of wrought magnesium alloys containing neodymium. Corr Sci 2012;58:145–51, http://dx.doi.org/10.1016/j.corsci.2012.01.021.
[18] Gu XN, Li N, Zheng YF, Kang F, Wang JT, Ruan L. In vitro study on equal channel angular pressing AZ31 magnesium alloy with and without back pressure. Mater Sci Eng A 2011;176:1802–6, http://dx.doi.org/10.1016/j.mseb.2011.04.003.
[19] Korchef A, Kahoul A. Corrosion behavior of commercial aluminum alloy processed by equal channel angular pressing. Int J Corros Scale Inhib 2013:1–11, http://dx.doi.org/10.1155/2013/983261.
[20] Son I, Nakano H, Oue S, Kobayashi S, Fukushima H, Horita Z. Pitting corrosion resistance of anodized aluminium alloy processed by severe plastic deformation. Mat Trans 2007;48:21–8, http://dx.doi.org/10.2320/matertrans.48.21.
[21] Song D, Ma A, Jian J, Lin P, Yang D, Fan J. Corrosion behavior of equal-channel-angular-pressed pure magnesium in NaCl aqueous solution. Corr Sci 2010;52:481–90, http://dx.doi.org/10.1016/j.corsci.2009.10.004.
[22] Ralston KD, Birbilis N. Effect of grain size on corrosion: a review. Corrosion 2010;66:1–13, http://dx.doi.org/10.5006/1.3462912.
[23] Sha G, Wang YB, Liao XZ, Duan ZC, Ringer SP, Langdon TG. Microestructural evolution of Fe-rich particles in an Al-Zn-Mg-Cu alloy during equal-channel angular pressing. Mat Sci Eng A 2010;572:4742–9, http://dx.doi.org/10.1016/j.msea.2010.04.041.
[24] Naderi M, Peterlechner M. The effect of pre-annealing on defects, microstructure and recrystallization of ultra-fine grained Al produced by high-pressure torsion. Mater Sci Eng A 2017;708:171–80, http://dx.doi.org/10.1016/j.msea.2017.09.126.
[25] Zhilyaev AP, Torres MJ, Cadena HD, Rodriguez SL, Calvo J, Cabrera JM. The effect of pre-annealing on the evolution of the microstructure and mechanical behavior of aluminum processed by a novel SPD method. Materials 2020;13:2361, http://dx.doi.org/10.3390/ma13102361.
[26] Abd-El-Aal MI, Sadawy MM. Influence of ECAP as grain refinement technique on microstructure evolution mechanical properties and corrosion behavior of pure aluminium. Trans Nonferrous Met Soc China 2015;25:3865–76, http://dx.doi.org/10.1016/S1003-6326(15)64034-1.
[27] Zaid B, Saidi D, Benzaid A, Hadji S. Effects of pH and chloride concentration on pitting corrosion of AA6061 aluminum alloy. Corr Sci 2008;50:1841–7, http://dx.doi.org/10.1016/j.corsci.2008.03.006.
[28] El Shayeb HA, Abd El Wahab FM, Zein El Abedin S. Electrochemical behavior of Al, Al–Sn, Al–Zn and Al–Zn–Sn alloys in chloride solutions containing indium ions. J Appl Electrochem 1999;29:473–80, http://dx.doi.org/10.1023/A:1003425306696.
[29] Thompson NG, Prayer JH. DC electrochemical test methods. Houston, Texas: NACE International ed; 1988.
[30] Trethewey K, Chamberlain J. Corrosion for science and engineering. first edition England: Longman Scientific & Technical; 1995.
[31] Silverman DC. Tutorial on cyclic potentiodynamic polarization technique. San Diego: Corrosion'98; 1998. p. 1–21.
[32] Abdulstaar M, Mhaede M, Wagner L, Wollmann M. Corrosion behaviour of Al 1050 severely deformed by rotatory swaging. Mater Design 2014;57:325–9, http://dx.doi.org/10.1016/j.matdes.2014.01.005.
[33] Ly R, Hartwing KT, Castaneda H. Influence of dynamic recrystallization and shear banding on localized corrosion of severely deformed Al-Mg-Si alloy. Materialia 2018;4:457–65, http://dx.doi.org/10.1016/j.mtla.2018.11.005.